EUROFUSION WPCD-CP(16) 16519

A Stegmeir et al.

The field line map approach for simulations of plasma edge/SOL turbulence

Preprint of Paper to be submitted for publication in
Proceedings of 26th IAEA Fusion Energy Conference

This work has been carried out within the framework of the EUROfusion Consortium and has received funding from the Euratom research and training programme 2014-2018 under grant agreement No 633053. The views and opinions expressed herein do not necessarily reflect those of the European Commission.

The field line map approach for simulations of plasma edge/SOL turbulence

A. Stegmeir[1], D. Coster[1], O. Maj[1], A. Ross[1] and K. Lackner[1]

[1]Max-Planck-Institute for Plasma Physics, 85748 Garching, Germany

Corresponding Author: Andreas.Stegmeir@ipp.mpg.de

Abstract:

The GRILLIX code is employed to study effects of geometry on turbulent structures. Based on the flux-coordinate independent approach (FCI), GRILLIX is highly flexible with respect to geometry and allows especially simulations across the separatrix with X-point(s) in diverted magnetic fusion devices. In contrast to the usually employed field/flux-aligned coordinates, there are no coordinate singularities at the separatrix/X-point(s) in the FCI approach, where parallel operators are discretised via a field line map. Being a paradigm for plasma turbulence and due to its simplicity, the Hasegawa-Wakatani model with inclusion of curvature is used for studies of basic behaviour of turbulent structures around the separatrix. We compare results obtained in geometries with closed magnetic flux surfaces, single null and double null configuration. In analogy to the resistive X-point mode, the results confirm that the strong magnetic shear around the X-point(s) leads to enhanced dissipation disconnecting the low field side with its unfavourable curvature from the high field side with favourable curvature.

1 Introduction

The flux-coordinate independent approach (FCI) [1, 2, 3, 4] has emerged as a promising and computationally efficient way to deal with geometrical problems related with a separatrix with X-point(s). The usually employed field/flux-aligned coordinates become singular at the separatrix/X-point(s) [5] and codes based on these coordinates have to provide some workaround or special treatment to resolve these coordinate singularities. Results from such codes concerning specifically the role of X-point(s) might therefore be debatable. The FCI approach is based on a cylindrical grid (R_i, Z_j, φ_k), i.e. Cartesian within poloidal planes, where discretisation of perpendicular operators is straight forward and simple. In order to computationally exploit the strong anisotropy of structures $\left(k_\parallel \ll k_\perp\right)$ the grid is coarsened in the toroidal direction and a field line map is used for the discretisation of parallel operators: For each grid point corresponding map points at the adjacent poloidal planes are computed via tracing along magnetic field lines, and discrete analogues of parallel operators are then constructed by employing a finite difference along magnetic field lines. An interpolation is thereby required to obtain values at

the map points. Finally, the FCI allows a natural treatment of regions where field/flux-aligned coordinates exhibit singularities, i.e. magnetic axis and separatrix with X-point(s) are not special but treated like any other grid point. The FCI has been applied successfully to hyperbolic [2] and parabolic [3, 6] problems, where especially the critical issue of numerical perpendicular diffusion was addressed which could be reduced drastically via application of conservative finite difference methods. Further subtle issues concern the effects of a distorted map and the treatment of boundary conditions within the FCI, which is discussed in [4, 7]. Furthermore, the FCI has already been applied to an ITG turbulence model in magnetic island geometry [8]. Finally the FCI approach has been proven to be a viable numerical approach and is currently employed or pursued in several codes like FENICIA [2], GRILLIX [3], FELTOR [9] and BOUT++ [10].

The code GRILLIX is adopted to the Hasegawa-Wakatani model [11] with inclusion of magnetic curvature (HWC). Though some assumptions of HWC are certainly not valid for typical edge/scrape-off layer (SOL) conditions, the simple HWC, being a aradigm for plasma turbulence, is suitable for a basic investigation about effects of geometry on turbulent structures. To elucidate the effect of the X-point we compare simulations with closed magnetic flux surfaces, a single null configuration with one X-point and a double null configuration with two X-points. We confirm a similar picture as described within the framework of the resistive X-point mode [12, 13]. Field aligned structures become strongly distorted near the X-point, which causes strong dissipation in this region. Ultimately the X-point acts like a barrier and tends to disconnect the outboard low field side, i.e. the region of unfavourable curvature, from the stabilizing high field side.

In section 2 we present the physical model and its implementation in GRILLIX. In section 3 we discuss the effect of an X-point on a field aligned turbulent structure and confirm this picture with simulations in section 4.

2 Model and its implementation in GRILLIX

2.1 Hasegawa-Wakatani model with curvature

Low temperatures in the scrape-off layer (SOL) justify the use of a fluid model. Moreover, structures are usually strongly anisotropic $k_\parallel \ll k_\perp$ and frequencies of interest ω are very slow compared to ion gyro motion of with frequency $\Omega_i = eB/(m_i c)$, which satisfies the requirements for a drift reduced fluid model [14]. However, the Hasegawa-Wakatani model is based on further simplifications which might certainly become questionable for typical edge/SOL conditions, i.e. magnetic induction, electron inertia and parallel streaming are neglected. Ions are assumed to be cold and electrons are assumed to be isothermal of constant temperature T_e. The remaining quantities are split into a background and fluctuation, e.g. for the density $n_e = n_0 + \tilde{n}$ obeying the ordering $\tilde{n} \ll n_0$, $\nabla_\perp n_0 \sim \nabla_\perp \tilde{n}$. Moreover, the assumption of a strong toroidal field against poloidal field allows to approximate perpendicular operators to act purely within poloidal planes, i.e. $\nabla_\perp = \mathbf{e}_R \partial_R + \mathbf{e}_Z \partial_Z$. The HWC equations describe finally the evolution of the perturbed density, the electro-

static potential and the parallel current in normalised form as:

$$\partial_t n + \frac{1}{B}\left[\phi, n + w_n\rho\right] = w_b\mathcal{C}(\phi - n) + \nabla\cdot\left[\mathbf{b}J_\parallel\right] + \nu_n\mathcal{D}_\perp(n) + S_n, \tag{1}$$

$$\partial_t\Omega + \frac{1}{B}\left[\phi, \Omega\right] = - w_b\mathcal{C}(n) + \nabla\cdot\left[\mathbf{b}J_\parallel\right] + \nu_v\mathcal{D}_\perp(\Omega) \tag{2}$$

$$J_\parallel = \sigma_\parallel^*\nabla_\parallel\left(n - \phi\right), \tag{3}$$

where time is measured in units of $L_\perp/c_s$ with $c_s = \sqrt{T_e/m_i}$ the sound speed and $L_\perp$ a characteristic background gradient length. Perpendicular scales are measured in units of ion sound radius $\rho_s = c_s/\Omega_i$ and parallel scales in units of major radius R_0. The magnetic field strength B is normalised against the magnetic field strength on axis and $\mathbf{b}$ is the magnetic field unit vector. We introduce the dimensionless parameter $\delta = \rho_s/L_\perp$ and normalise the density fluctuation according to $n := \delta^{-1}\tilde{n}/n_0$, the electrostatic potential according to $\phi := \delta^{-1}e\tilde{\phi}/T_e$ with the vorticity defined as $\Omega := \nabla_\perp^2\phi$, and the parallel current according to $J_\parallel = \delta^{-1}\tilde{J}_\parallel/(en_0c_s)$. The Jacobi brackets $[\phi, f] := \partial_R\phi\partial_Z f - \partial_Z\phi\partial_R f$ represent advection with $\mathbf{E}\times\mathbf{B}$ velocity and $\mathcal{C} := 2\partial_Z$ represents curvature terms. Perpendicular dissipation is modelled via high order diffusion $D_\perp := \nabla_\perp^6$ which shall strongly dissipate structures on the grid scale but leave larger structures unaffected. The background density is assumed to be constant on flux surfaces with ρ a normalized flux label. The parameter w_n controls the strength of the background density gradient and $w_b := L_\perp/R_0$ the strength of curvature. The dimensionless parallel conductivity is defined as $\sigma_\parallel^* := c_s m_i L_\perp/(0.51\nu_e m_e R_0^2)$, where ν_e is the collision frequency. Finally the parameters ν_n and ν_v control the strength of perpendicular dissipation. Since turbulence tends to remove its drive, i.e. the density gradient, we introduce a source/sink terms S_n acting in buffer zones near the inner and outer limiting flux surfaces which damps the zonal averaged density fluctuations and the zonal averaged potential.

At the intersection of magnetic field lines with divertor plates the parallel current is assumed to vanish, so the divertor plates can be regarded as perfect insulators, and homogeneous Neumann boundary conditions are applied for the remaining quantities in the direction normal to the divertor. Homogeneous Dirichlet boundary conditions are applied for n, ϕ, Ω at the inner and outer limiting flux surfaces.

The Hasegawa-Wakatani model (originally formulated without curvature terms [11]) describes resistive drift-ballooning turbulence. It is a very well established paradigm for plasma turbulence and is therefore often used for basic studies on plasma turbulence.

2.2 Implementation

A cylindrical grid is employed in GRILLIX, where only those points are retained in memory which lie in between two limiting flux surfaces ψ_{min} and ψ_{max}. The Arakawa scheme [15] is used for discretisation of the Jacobi bracket and standard second order finite difference methods for the discretisation of the remaining perpendicular operators. By inserting Ohm's law, i.e. eq. (3), into eqs. (1) and (2) the parallel terms appear only as $\sigma_\parallel^*\nabla\cdot\left[\mathbf{b}\nabla_\parallel\left(n - \phi\right)\right]$. The discretisation of the parallel diffusion operator via a conservative finite difference scheme, which exhibits very low numerical perpendicular diffusion,

is discussed and benchmarked isolatedly in detail in [3, 4] and we use the **S-3X2** scheme from [4] which employs a third order bipolynomial interpolation. The treatment of the boundary conditions is discussed in [4] as well. A third order stiffly-stable splitting method is used for time advance [16], where the parallel current terms are treated fully implicitly in order to ensure numerical stability. We refer to [17] for further material on verification and benchmarks of the HWC model within GRILLIX.

GRILLIX is MPI-parallelized over the toroidal direction and within each poloidal plane OpenMP parallelisation, respectively multithreaded libraries are employed. The implicitely treated parallel dynamics is treated via a parallel GMRES solver and the polarisation, i.e. the elliptic problem $\Omega = \nabla_\perp^2 \phi$, via a parallel sparse direct solver.

3 Theoretical picture for X-point

To illustrate the effect of an X-point on a field aligned structure, we consider a simple model geometry as illustrated in fig. 1, where z is a coordinate along a reference magnetic field which approaches the X-point in the limit $z \to \infty$. With $z = 0$ we identify the outboard midplane region, where the strongest drive for the turbulence is located. x and y are coordinates perpendicular to the reference magnetic field line. We assume that the outboard midplane region is shearless and separated sharply from the X-point region at $z = z_x$. The (normalized) magnetic field is:

$$\mathbf{B} = \mathbf{e}_z + \alpha \left[x\mathbf{e}_x - y\mathbf{e}_y \right] \Theta(z - z_x), \quad (4)$$

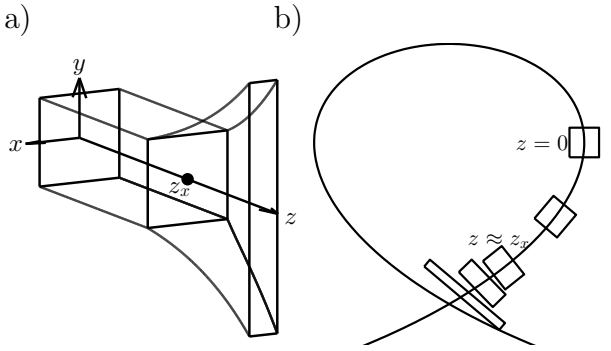

FIG. 1: a) Distortion of flux box around reference magnetic field line approaching X-point at $z \to \infty$. $z = 0$ is identified with outboard midplane region and at $z = z_x$ X-point region is entered. b) Schematic view of flux box in poloidal projection in tokamak geometry.

with α a parameter expressing the shear around the X-point and Θ the Heavyside step function. Field lines can easily be traced and the perpendicular components of the wave vector of a field aligned structure $\left(k_\parallel \approx 0\right)$ obeys along z [18]:

$$k_x(z) = k_{x0} \exp(\alpha \xi(z)), \quad k_{y0}(z) = k_{y0} \exp(-\alpha \xi(z)), \quad (5)$$

where $\xi(z) = (z - z_x)\,\Theta\,(z - z_x)$ and k_{x0}, k_{y0} are the perpendicular wave vector components at $z = 0$. Eqs. (5) imply that a field aligned structure becomes strongly distorted around the X-point and the absolute value of its perpendicular wave vector component grows strongly as it approaches closer to the X-point, i.e. $k_\perp^2(z) \underset{\xi(z) \gg \alpha}{\longrightarrow} k_{0x}^2 \exp(2\alpha\xi(z))$. We therefore expect operators with the highest $k_\perp$ dependence to be dominant in the vicinity of X-point(s) and within the employed HWC model perpendicular dissipation scales with

$k_\perp^6$. Even if the strong $k_\perp^6$ dependence arises here from an ad-hoc introduced hyperdiffusion model the perpendicular dissipation would still be dominant for a $k_\perp^2$ dependence.

Turbulence is mainly driven at in the outboard midplane region and via parallel currents field aligned structures are established. However, around the X-point these structures become strongly distorted and perpendicular dissipation becomes at some point dominant over the parallel dynamics. Finally the X-point disconnects structures at the outboard midplane region from the stabilizing high field side [12, 13].

4 Simulations

We try to confirm the picture given in the previous section by carrying out simulations with GRILLIX. The normalized magnetic field is given in terms of an axisymmetric poloidal flux function as $B = \nabla\varphi + \nabla\varphi \times \nabla\psi/I_0$, for which we consider an up-down symmetric and asymmetric configuration with the constant $I_0 = 2\pi \cdot 3.50$ [19]:

$$\begin{aligned}\psi_S(R,Z) =& 1.56 - 1.14R^2 - 0.15RJ_1(3.30R) - 3.70RY_1(3.30R)\\ &- 2.56RJ_1(2.64R)\cos(1.98Z) + 2.00RJ_1(1.98R)\cos(2.64Z)\\ &+ 1.21RJ_1(0.33R)\cos(3.28Z) - 2.13RJ_1(3.86R)\cosh(2.00Z)\\ \psi_A(R,Z) =& \Psi_S(R,Z) + 0.65RZJ_1(3.30R) + 1.32RJ_1(2.64R)\sin(1.98Z) - 0.91\sin(3.30Z),\end{aligned}$$

where the coefficients are given with two significant digits and J_n, Y_n are Bessel functions of the first respectively second kind. The magnetic axis and X-points for the symmetric configuration are at the positions $(1.75, 0)$ respectively $(0.86, \pm 0.42)$. For the asymmetric equilibrium the magnetic axis is at $(1.77, -0.23)$ and an X-point at (0.84,-0.37). The normalised flux label is introduced as $\rho := \sqrt{(\psi - \psi_0)\,/\,(\psi_X - \psi_0)}$, with ψ_0, ψ_X the magnetic flux on the magnetic axis respectively on the separatrix.

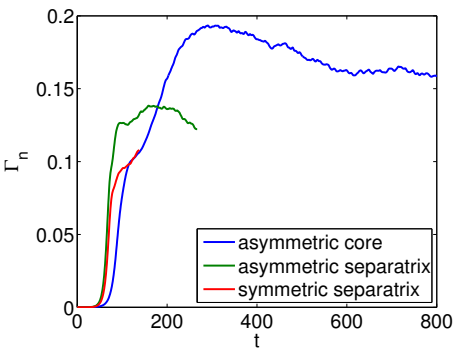

FIG. 2: Time trace of average radial particle transport $\Gamma_n = \int n\mathbf{v}_\rho\, dV/V$. Due to computational cost only the case 1 could yet be carried to a saturated state

As parameters for the simulations we choose $\rho_s/R_0 = 3.13 \cdot 10^{-4}$. We set the background density gradient length at the outboard midplane side as the normalisation length, i.e. $L_\perp/R_0 = w_b = 0.022$ with $w_n = -700$. Finally, we set the parameter $\sigma_\parallel^* = 1$. We employ $N_{pol} = 20$ poloidal planes with a perpendicular resolution of $h = 0.66$ and set the dissipation coefficients to $\nu_n = \nu_v = 1 \cdot 10^{-3}$. The buffer zones near the inner and outer limiting flux surfaces have a radial extension of 10% with a Gaussian envelope. Due to computational costs it was not possible to perform convergence checks for the particular cases discussed here, but these parameters were proven to yield converged results for computationally less expensive smaller cases

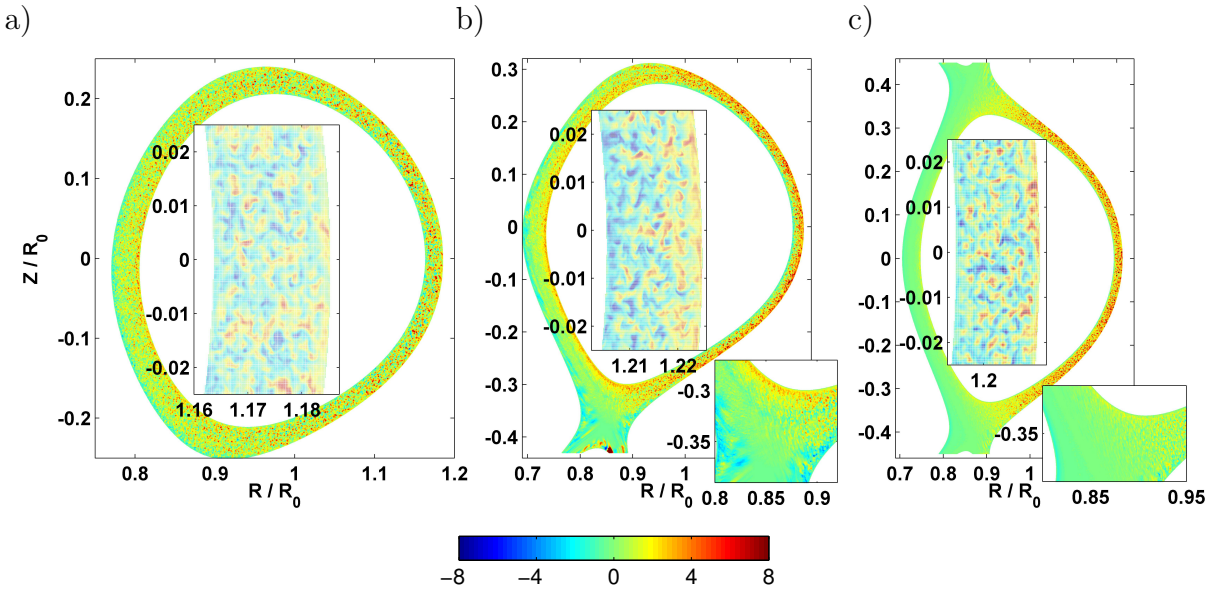

FIG. 3: Snapshots of density fluctuations n at plane $\varphi = 0$. a) Case 1 at $t = 300$, b) case 2 with single X-point at $t = 260$ and c) case 3 with two X-points at $t = 135$. Insets show outboard midplane region and X-point region enlarged.

with circular flux surfaces [17]. Moreover, our studies here focus on qualitative but not yet quantitative effects arising from X-point(s).

We investigate three cases: A simulation in the asymmetric configuration on closed field lines with $\rho \in [0.75, 0.85]$ (case 1), a simulation in the asymmetric configuration in the range $\rho \in [0.94, 1.03]$ with a single X-point in the domain (case2), and a simulation in the symmetric configuration in the range $\rho \in [0.94, 1.03]$ with two X-points in the domain (case 3). The simulations were initialized with small random noise in the density perturbation and in fig. 2 we show time traces for the volume averaged radial particle transport. Due to limitations arising from long runtimes we were only able to carry out case 1 to a fully saturated state. However, since we are yet only interested in a qualitative picture it is sufficient to consider in the following the timepoints where the transition to a non-linear state occurs, i.e. $t = 300$ for case 1, $t = 270$ for case 2 and $t = 135$ for case 3. Snapshots of density fluctuations at these time points are shown in fig. 3. The strongest drive and therefore the largest fluctuations are in the outboard midplane region. For case 1 these fluctuations are mediated via parallel currents to the stabilizing high field side. In case 3 the two X-points completely disconnect in the parallel direction the high field side from the low field side and no fluctuations can be observed on the high field side. Due to the presence of only one X-point there is only a partial disconnection of the high and low field side in case 2.

In order to get an impression on the parallel structure of the fluctuations we show the non-adiabaticity $n - \phi$ on flux surfaces for the three cases in fig. 2. In case 1 the parallel extension of fluctuations is very long and inboard and outboard side are connected. In case 3 the two X-points act like a barrier and disconnect the outboard side, where fluctuations

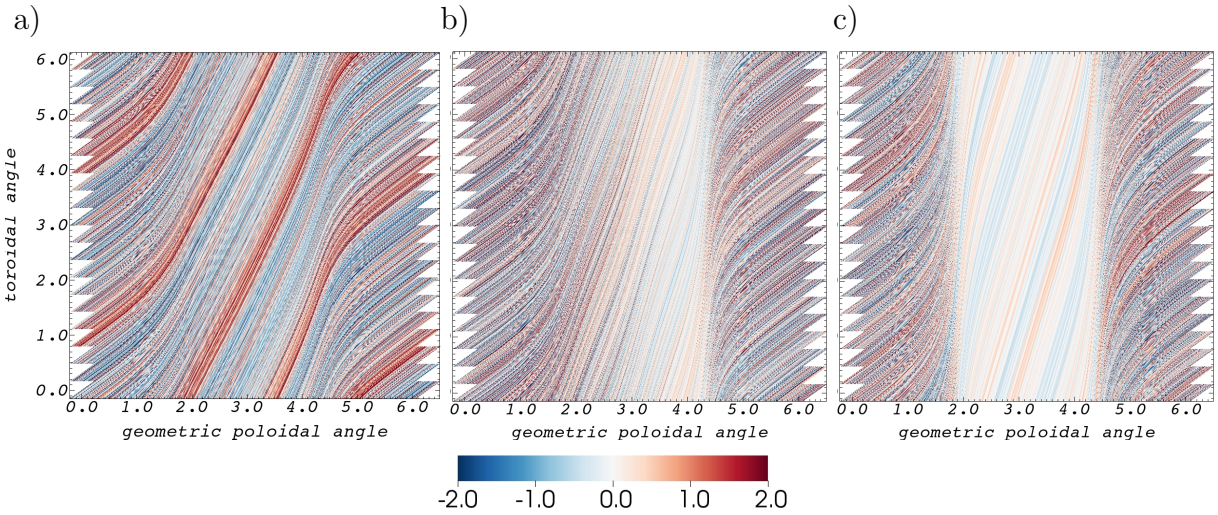

FIG. 4: Nonadiabiticity $n - \phi$ (zonal component has been removed) on flux surface for a) case 1 at $\rho = 0.8$, b) case 2 at $\rho = 0.98$ and c) case 3 at $\rho = 0.98$. Y-axis denotes toroidal angle φ and x-axis denotes geometric poloidal angle $\tan\theta = (Z - Z_0)/(R - R_0)$, i.e. outboard midplane is at $\theta = 0, 2\pi$, top at $\theta = \pi/2$ inboard midplane at $\theta = \pi$ and bottom at $\theta = 3\pi/2$. In the neighbourhood of the X-point(s), i.e. $\theta \sim 4.5$ in b) and $\theta \sim 1.8, 4.5$ in c), field lines are strongly bent and run nearly toroidally.

are located, from the stabilizing inboard side. In case 2 the X-point also acts like a barrier in the bottom region, but fluctuations can reach the inboard side via the top. These results confirm the theoretical picture from the previous section very well.

5 Discussion

We employed the code GRILLIX to study the role of the X-point on turbulent structures. Since GRILLIX is based on the flux-coordinate independent approach, the separatrix and X-point(s) are numerically not special but treated like any other grid point. Being a paradigm for plasma turbulence, the Hasegawa-Wakatani equations served as a physical model. Due to the strong magnetic shear, dissipation becomes dominant in the vicinity of the X-point. The X-point ultimately tends to disconnect structures along the parallel direction, and fluctuations remain located to the outboard plane where the curvature is unfavourable. Simulations carried out with GRILLIX confirmed this picture, which has also been found in experiment [20, 21].

6 Acknowledgements

This work was carried out using the HELIOS supercomputer system at Computational Simulation Centre of International Fusion Energy Research Centre (IFERC-CSC), Aomori, Japan, under the Broader Approach collaboration between Euratom and Japan, implemented by Fusion for Energy and QST. This work has been carried out within the framework of the EUROfusion Consortium and has received funding from the Euratom

research and training programme 2014-2018 under grant agreement No 633053. The views and opinions expressed herein do not necessarily reflect those of the European Commission. The support from the EUROfusion Researcher Fellowship programme under grant number AWP16-ERG-MPG/Stegmeir is gratefully acknowledged.

References

[1] M. Ottaviani. *Phys. Lett. A*, 375:1677, 2011.

[2] F. Hariri and M. Ottaviani. *Comput. Phys. Commun.*, 184:2419, 2013.

[3] A. Stegmeir et al. *Comput. Phys. Commun*, 198:139, 2016.

[4] A. Stegmeir et al. *submitted to Comput. Phys. Commun*, 2016.

[5] W. D. D'haeseleer, W. N. G. Hitchon, J. D. Callen, and J. L. Sohet. *Flux Coordinates and Magnetic Field Structure*. Springer Series in Computational Physics. 1990.

[6] A. Stegmeir et al. *Contrib. Plasm. Phys.*, 54:549, 2014.

[7] P. Hill et al. *arXiv:1608.02416v1 [physics,plasm-ph]*, 2016.

[8] F. Hariri others. *Phys. Plasmas*, 21:082509, 2014.

[9] M. Held et al. *Comput. Phys. Commun*, 199:29, 2016.

[10] B. D. Dudson et al. *arXiv [physics.plasm-ph]*, 1602.06747v1, 2016.

[11] A. Hasegawa and M. Wakatani. *Phys. Rev. Lett.*, 50:682, 1983.

[12] J.R. Myra et al. *Phys. Plasmas*, 7:4622, 2000.

[13] X.Q. Xu et al. *Phys. Plasmas*, 7:1951, 2000.

[14] A. Zeiler et al. *Phys. Plasmas*, 4:2134, 1997.

[15] A. Arakawa. *J. Comput. Phys.*, 135:103, 1997.

[16] G. Karniadakis et al. *J. Comput. Phys.*, 97:414, 1991.

[17] A. Stegmeir. *GRILLIX: A 3D turbulence code for magnetic fusion devices based on a field line map*. PhD thesis, Technische Universität München, 2015.

[18] D. Farina et al. *Nucl. Fusion*, 33:1315, 1993.

[19] P. J. Mc Carthy. *Phys. Plasmas*, 6:3554, 1999.

[20] M. Endler. *Experimentelle Untersuchung und Modellierung elektrostatischer Fluktuationen in den Abschlschichten des Tokamak ASDEX und des Stellarators Wendelstein 7-AS*. IPP report, 1994.

[21] V. Nikolaeva et al. *43rd EPS Conference on Plasma Physics*, P1.038, 2016.